Electronic Supplementary Material (ESI) for Catalysis Science & Technology.

Supporting information

Ring-opening of furfuryl alcohol to pentanediol with extremely high selectively over Cu/MFI catalysts with balance Cu^0-Cu^+ and Brønsted acid sites

Dengfeng Dai[a], Chao Feng[a], Minmin Wang[a], Qingzhou Du[a], Dandan Liu[a,b]*, Yuan Pan[a]*, Yunqi Liu[a]*

[a]State Key Laboratory of Heavy Oil Processing, China University of Petroleum (East China), Qingdao 266580 (China), liuyq-group@upc.edu.cn, panyuan@upc.edu.cn

[b]College of New Energy, China University of Petroleum (East China), Qingdao 266580 (China), liudandan@upc.edu.cn

*Corresponding author

1.1 Characterization techniques

H_2-TPR experiments of the samples were carried out on the AutoChem HP 2950 chemisorption analyzer (Micromeritics). The samples (100 mg) were pretreated under Ar gas at 350 °C for 1 h and conducted with 5 vol% H_2/Ar at a heating rate of 10 °C/min from room temperature to 800 °C.

Cu loadings and SiO_2/Al_2O_3 ratios of all the catalysts were determined by inductively coupled plasma atomic emission spectroscopy (ICP-OES) on an IRIS Intrepid II XSP instrument (Thermo Electron Corporation).

CO in situ diffuse reflectance infrared Fourier transform spectra (CO-DRIFT) measurements on the reduced Cu/Beta zeolites were conducted on a spectrometer (Bruker vertex 70) with 64 scans at a resolution of 4 cm^{-1}. The self-supporting pellets of the catalyst samples were placed into the reaction chamber, pretreated under helium flowing at 250 °C for 40min, and subsequently cooled to 25 °C capture background. Then, CO (10% CO/90 % He) was introduced into the DRIFT cell at a gas flow rate of 20 mL/min; The DRIFTS spectra were obtained after 5min stabilization.

1.2 Computational details

All calculations were performed using the density functional theory (DFT) technique using the Vienna ab initio simulation package (VASP). Spin-polarized calculations were performed using the generalized gradient approximation (GGA) combined with the Perdew–Burke–Ernzerhof (PBE) method to determine the exchange and correlation energies. The projector-augmented wave (PAW) method was used to represent the core–valence electron interactions. The typical plane-wave cutoff energy was 400 eV for basis-set expansion. For geometry optimization calculations, forces were converged below 0.03 eV/Å. The SCF convergence energy was 1×10^{-4} Ha. A 1 × 1 × 1 k-point mesh was used to perform all the calculations.

The binding energy (E_{ads}) was calculated as follows:

$$E_{ads} = E_{adsorbate+surface} - E_{surface} - E_{gas}$$

where $E_{surface}$ is the clean surface relaxation energy of the surface slab, E_{gas} is the energy of a free gas molecule under conditions of vacuum, and $E_{adsorbate+surface}$ is the energy of the composite system. As the calculations are performed at 0 K at a fixed cell volume,

the differences in the Gibbs free energy should equal the differences in the total energy. By this definition, a negative value of Eads corresponds to exothermic and spontaneous adsorption processes.

1.3 Figures and Tables

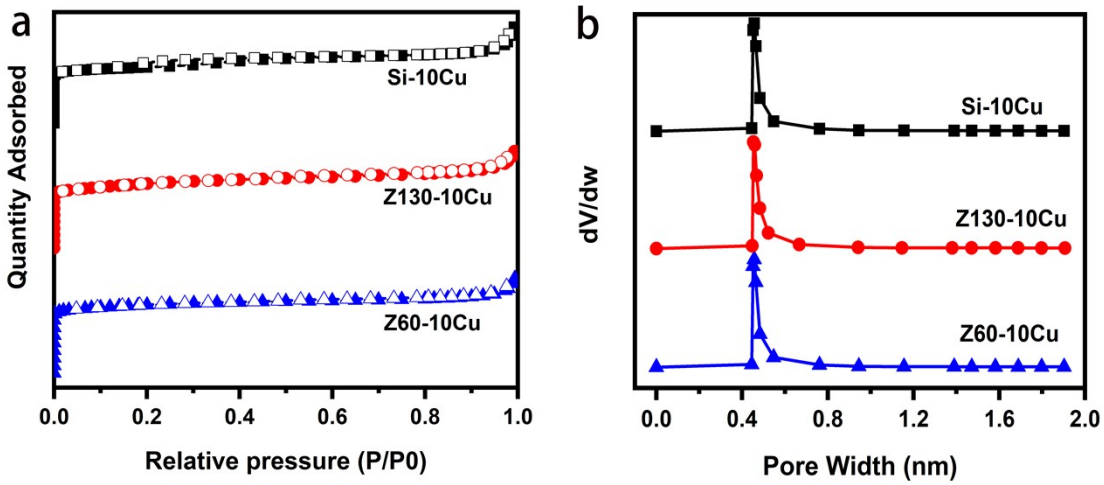

Figure S1. (a): full nitrogen sorption isotherms of the Z60-10Cu, Z130-10Cu, and Si-10Cu; (b): pore size distribution of the Z60-10Cu, Z130-10Cu, and Si-10Cu.

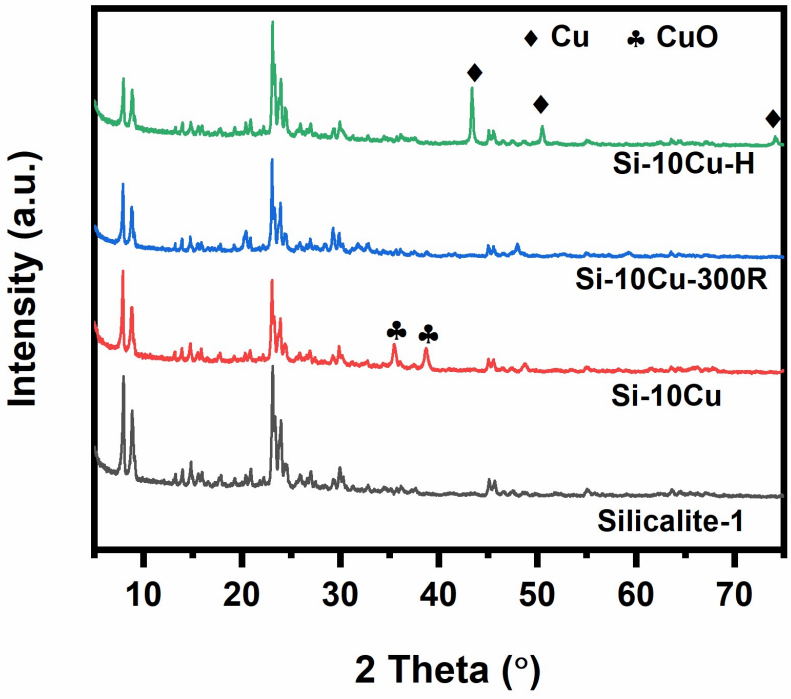

Figure S2. XRD patterns of the Silicalite-1, Si-10Cu, Si-10Cu-300R, Si-10Cu-H.

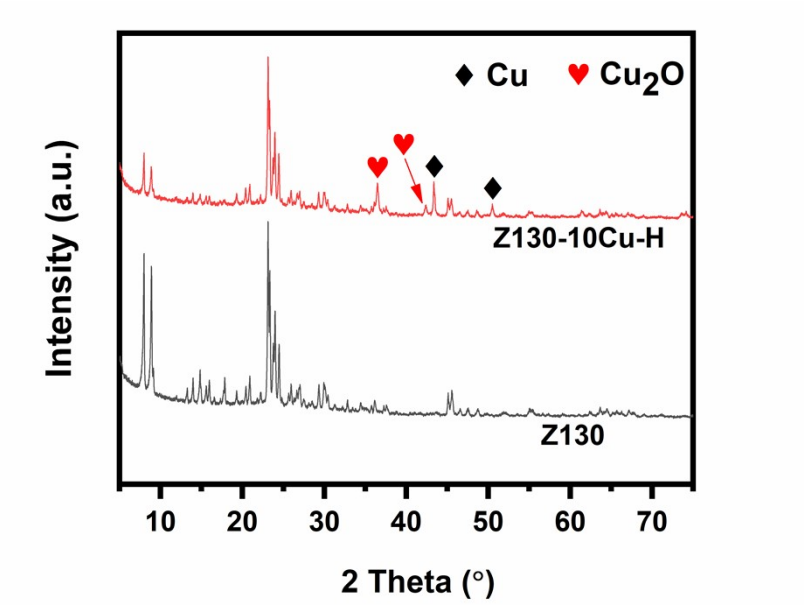

Figure S3. XRD patterns of the Z130, Z130-10Cu-H.

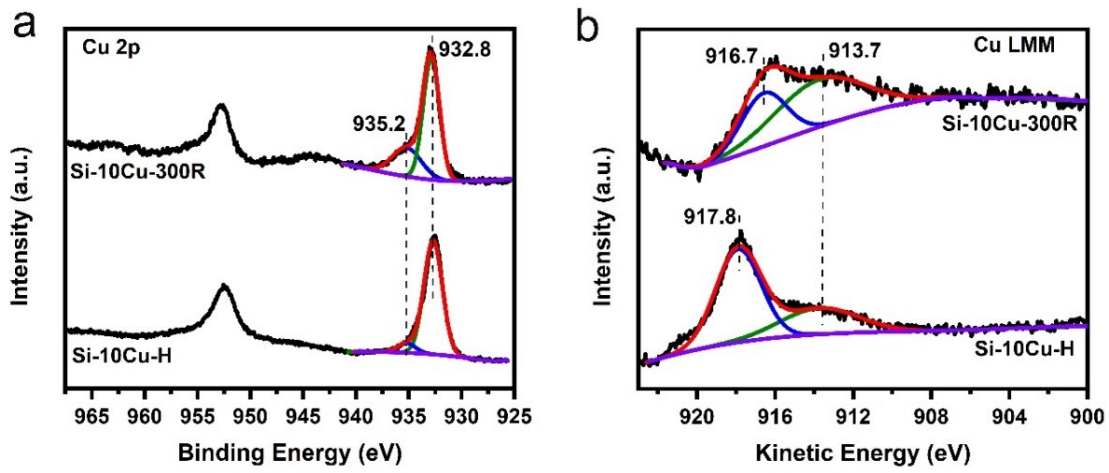

Figure S4. (a): Cu 2p XPS spectrum of Si-10Cu-300R and Si-10Cu-H; (b): Cu LMM XAES spectrum of Si-10Cu-300R and Si-10Cu-H;

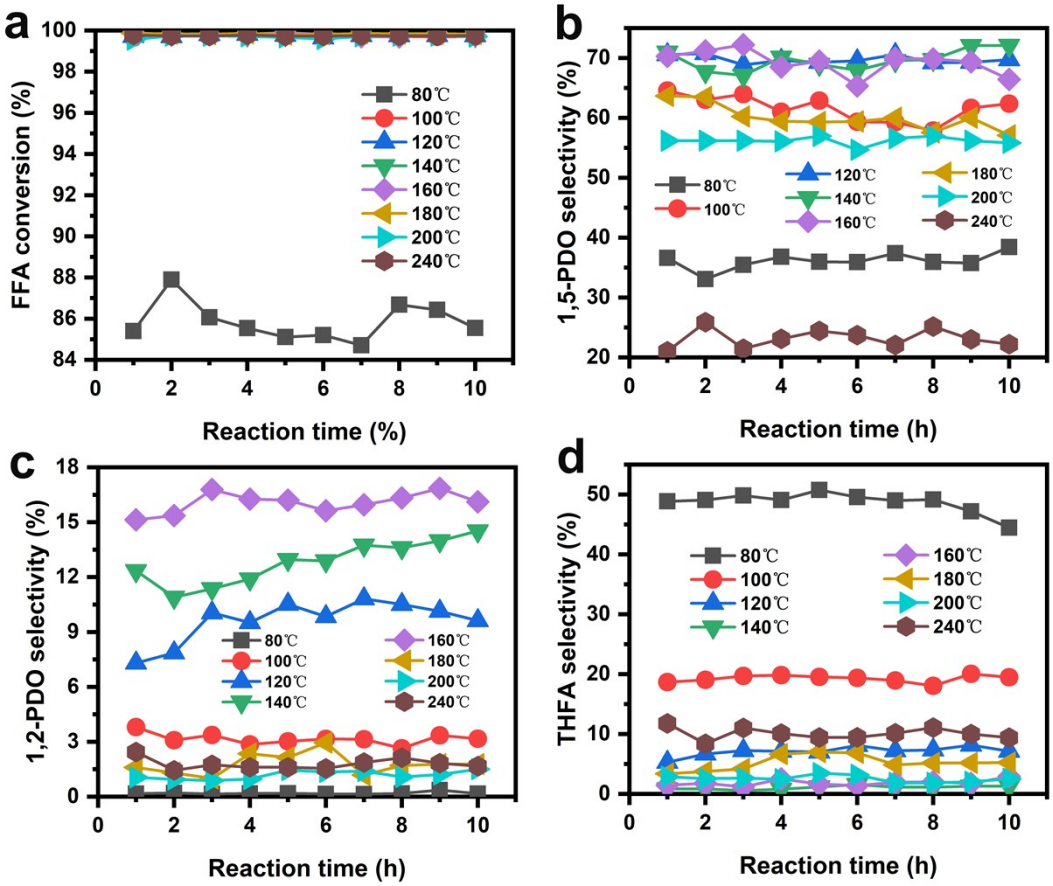

Figure S5. The effect of reaction temperatures on ring-opening of FFA over Z60-10Cu-300R catalyst

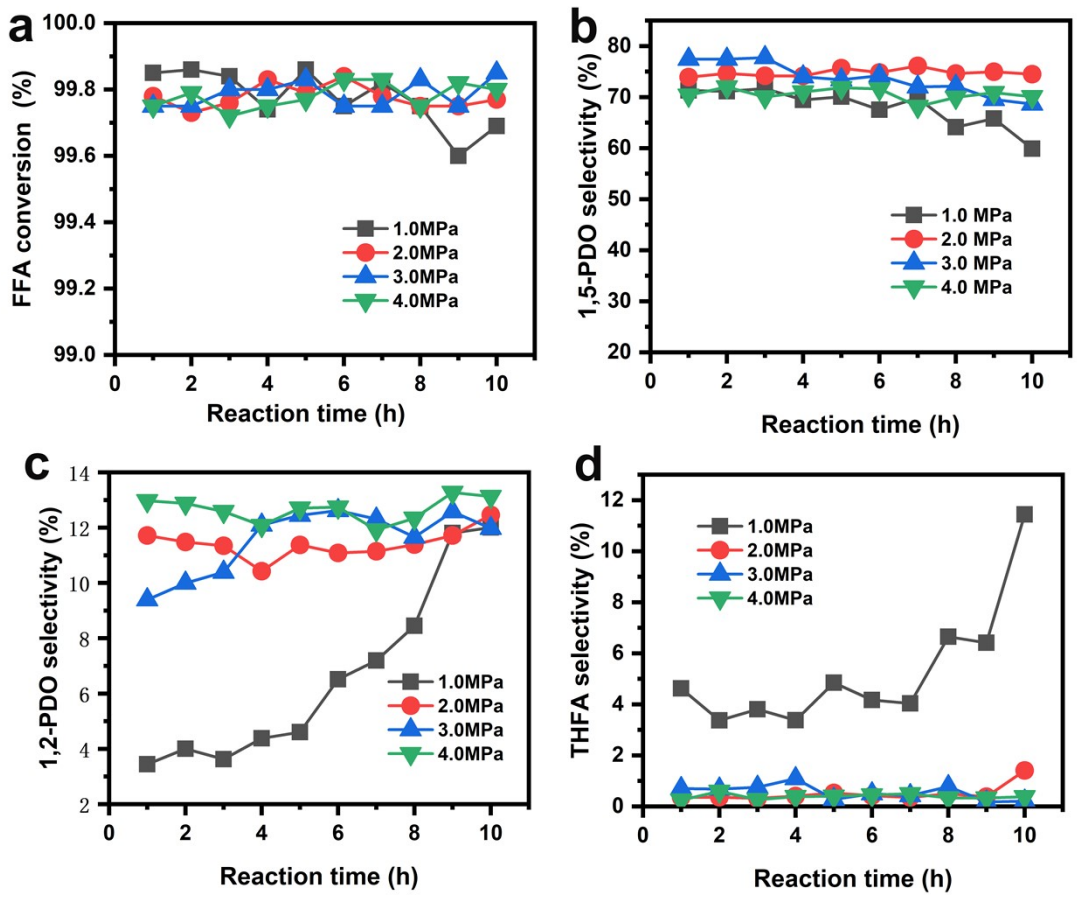

Figure S6. The effect of reaction pressure on ring-opening of FFA over Z60-10Cu-300R catalyst

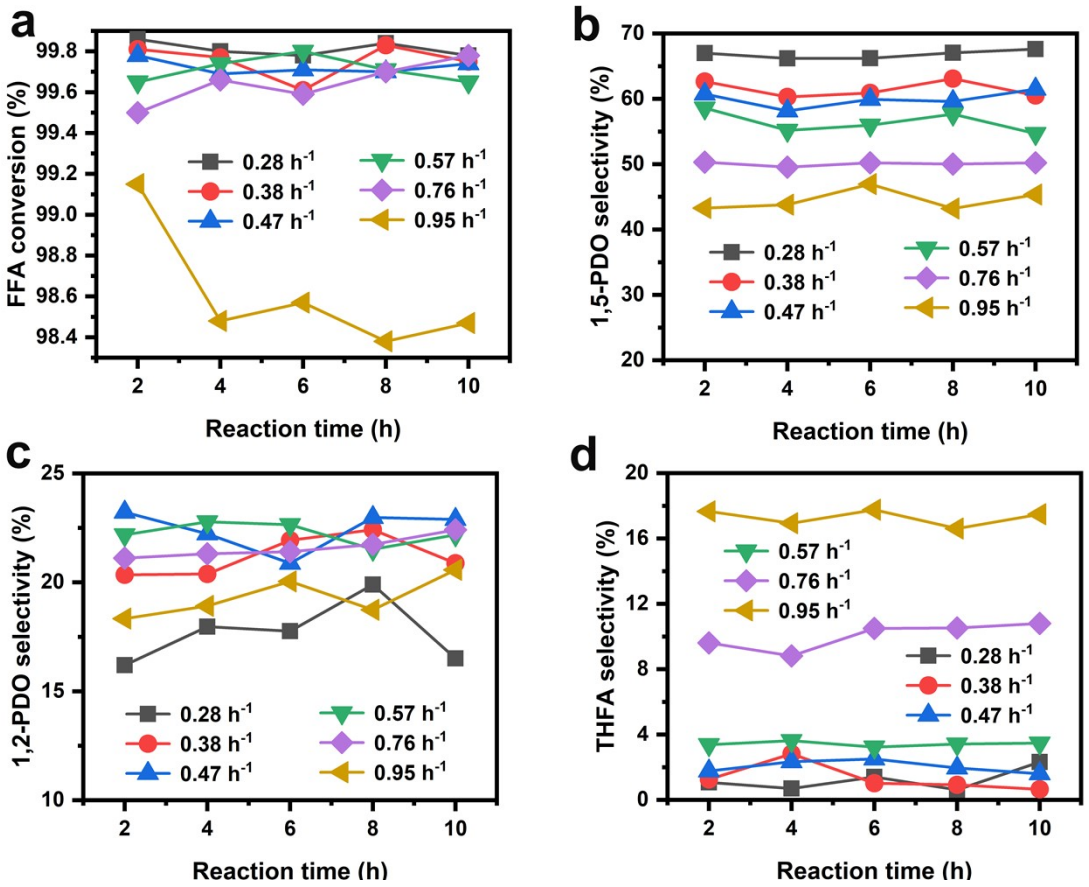

Figure S7. The effect of WHSV on ring-opening of FFA over Z60-10Cu-300R catalyst

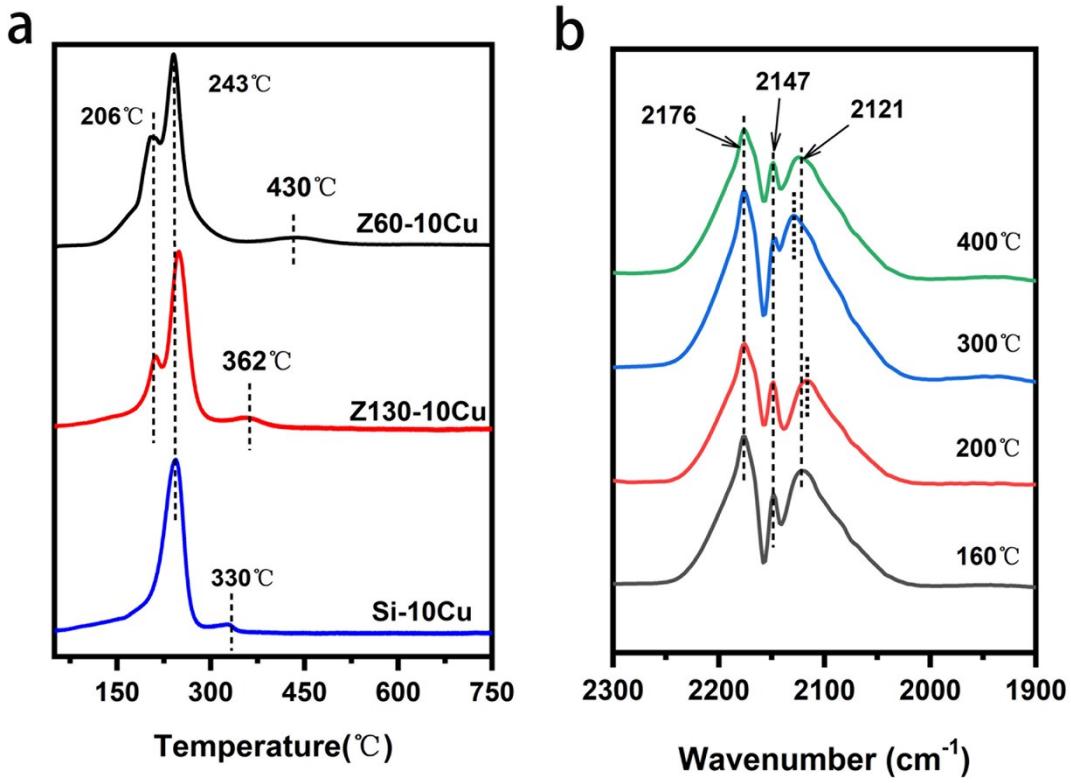

Figure S8. (a): H_2-TPR profile of Z60-10Cu, Z130-10Cu, Si-10Cu; (b) CO-DRIFT profiles of Z60-10Cu-160℃, Z60-10Cu-200℃, Z60-10Cu-300℃, Z60-10Cu-400℃. Note: Z60-10Cu-160℃ sample was Z60-10Cu activated by hydrogen at 160 ℃ for 0.5 h.

The H_2-TPR profile of the Z60-10Cu catalyst displayed two main peaks at 206℃ and 243℃, which should be ascribed to the reduction of highly dispersed CuO and the reduction of CuO with small size, indicating the uniformly distribution of the small Cu particles[1,2], and was validated by the HRTEM result. A broad signal at ~430℃ was observed in the Z60-10Cu, as a result of strong interaction between Cu species and support[3,4]. Similar reduction peaks also appear in the Z130-10Cu and Si-10Cu catalyst, but the reduction peak at high-temperature stage is slightly lower than Z60-10Cu, It may be related to the density of hydroxyl group and Si(OH)Al on the support surface. As we all know, hydroxyl group and Si(OH)Al can be used as anchor sites to fix the active metal and enhance the metal-support interaction[5,6]. Especially the MFI support after ammonia treatment may increase anchor sites.

The CO-DRIFT spectroscopy of different reduction temperature presented three characteristic bands at ~2176 cm^{-1}, ~2147 cm^{-1}, and ~2121 cm^{-1}, can be ascribed to the symmetric and antisymmetric vibrations of Cu^{+}–$(CO)_2$ species and Cu^{+}–CO species[7-9], respectively. Owing to the weaker interaction between Cu^{2+},Cu^{0} and CO, the corresponding Cu^{2+}-CO and Cu^{0}-CO complexes are very unstable and difficult to detect, particularly when they are in copresence with Cu^{+} sites[9].

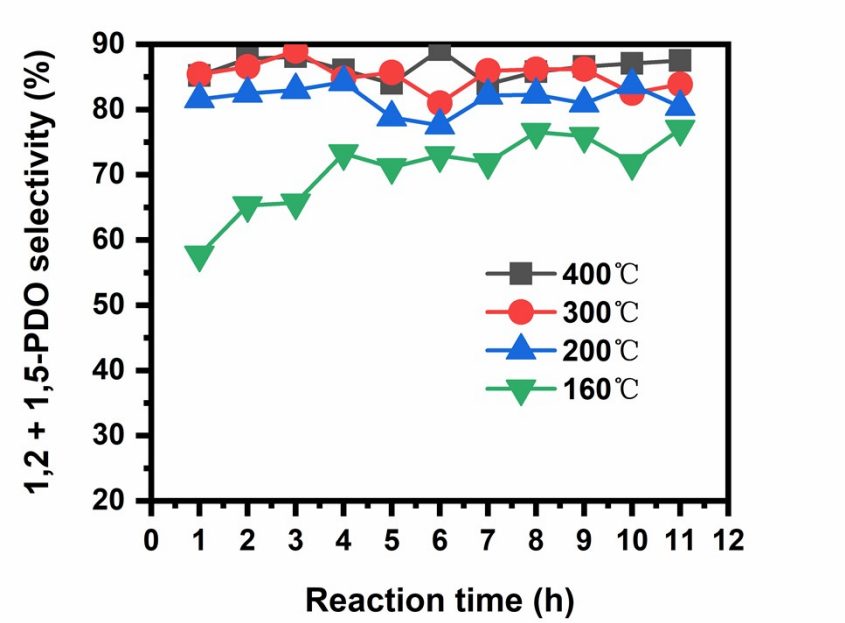

Figure S9. The selectivity of 1,2 and 1,5-PDO after being reduced at a different temperature, catalysts performance test condition: 160 ℃ and 2.5 MPa of 40 ml/min H_2, 2 wt% FFA, ETOH as solvent, 0.2 ml/min.

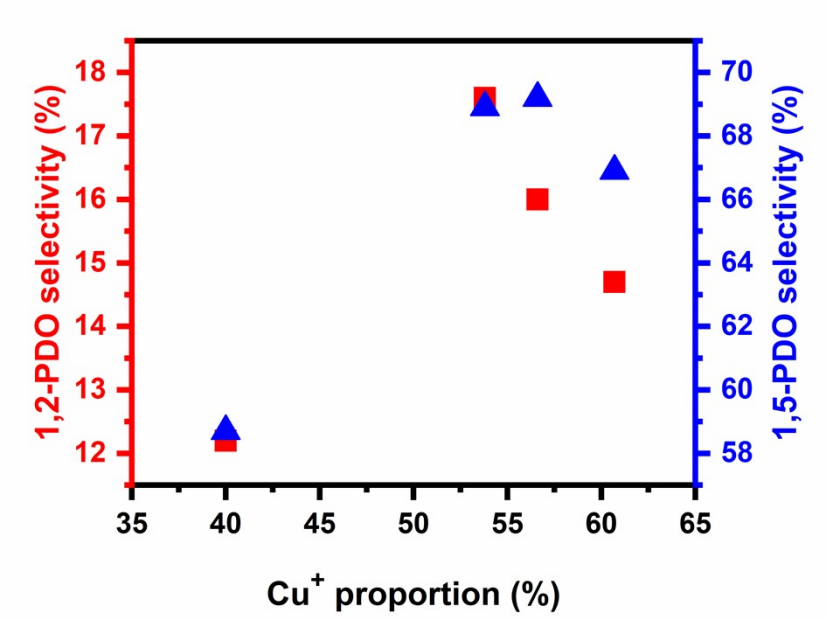

Figure S10. Correlation of Cu^{+} proportion and PDO selectivity.

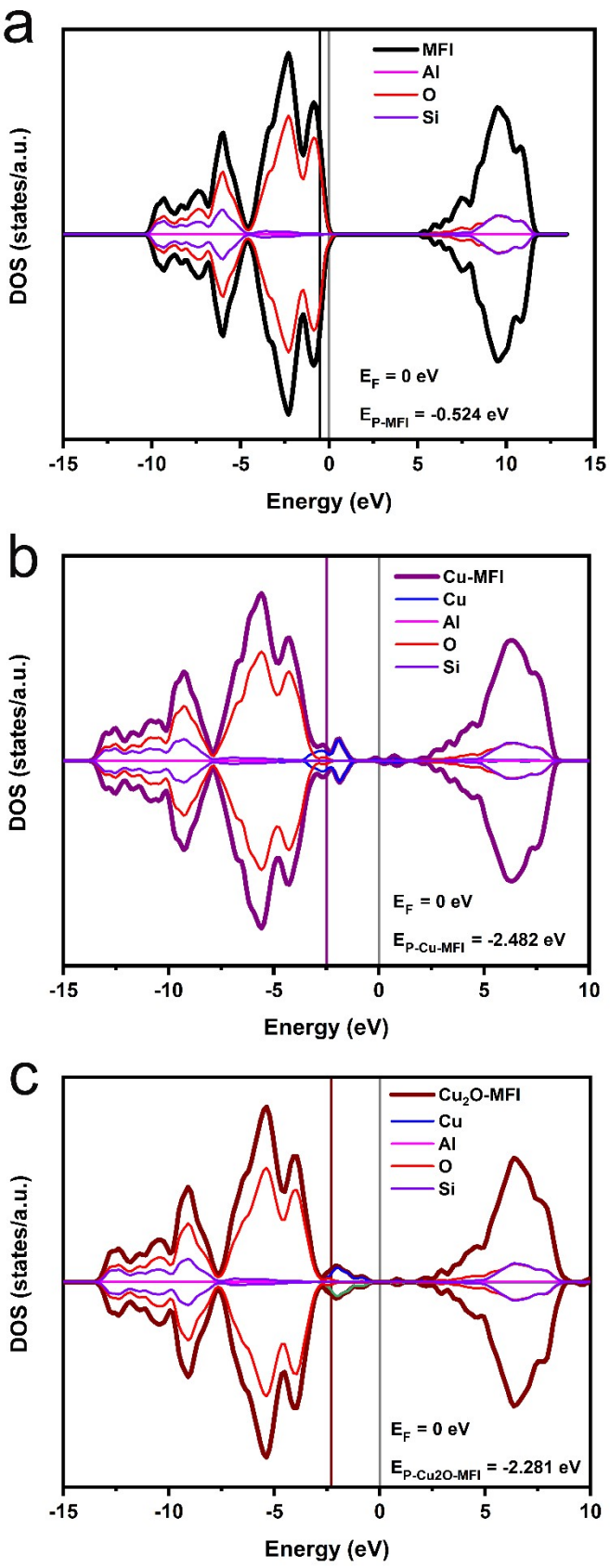

Figure S11. Density of states (DOS) for (a): MFI, (b): Cu-MFI, and (c): Cu_2O-MFI

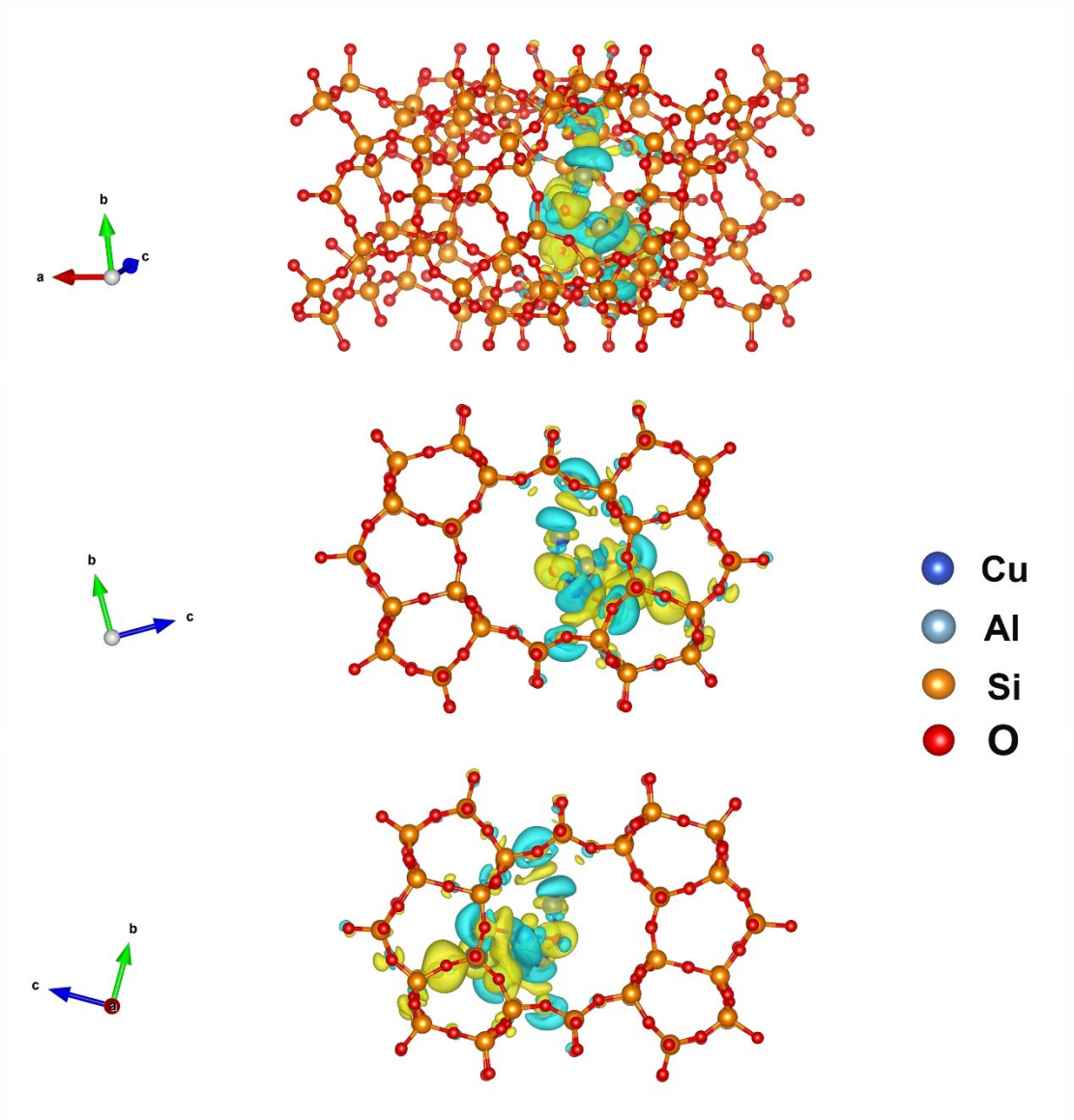

Figure S12. Differential charge density diagram of Cu_2O-MFI

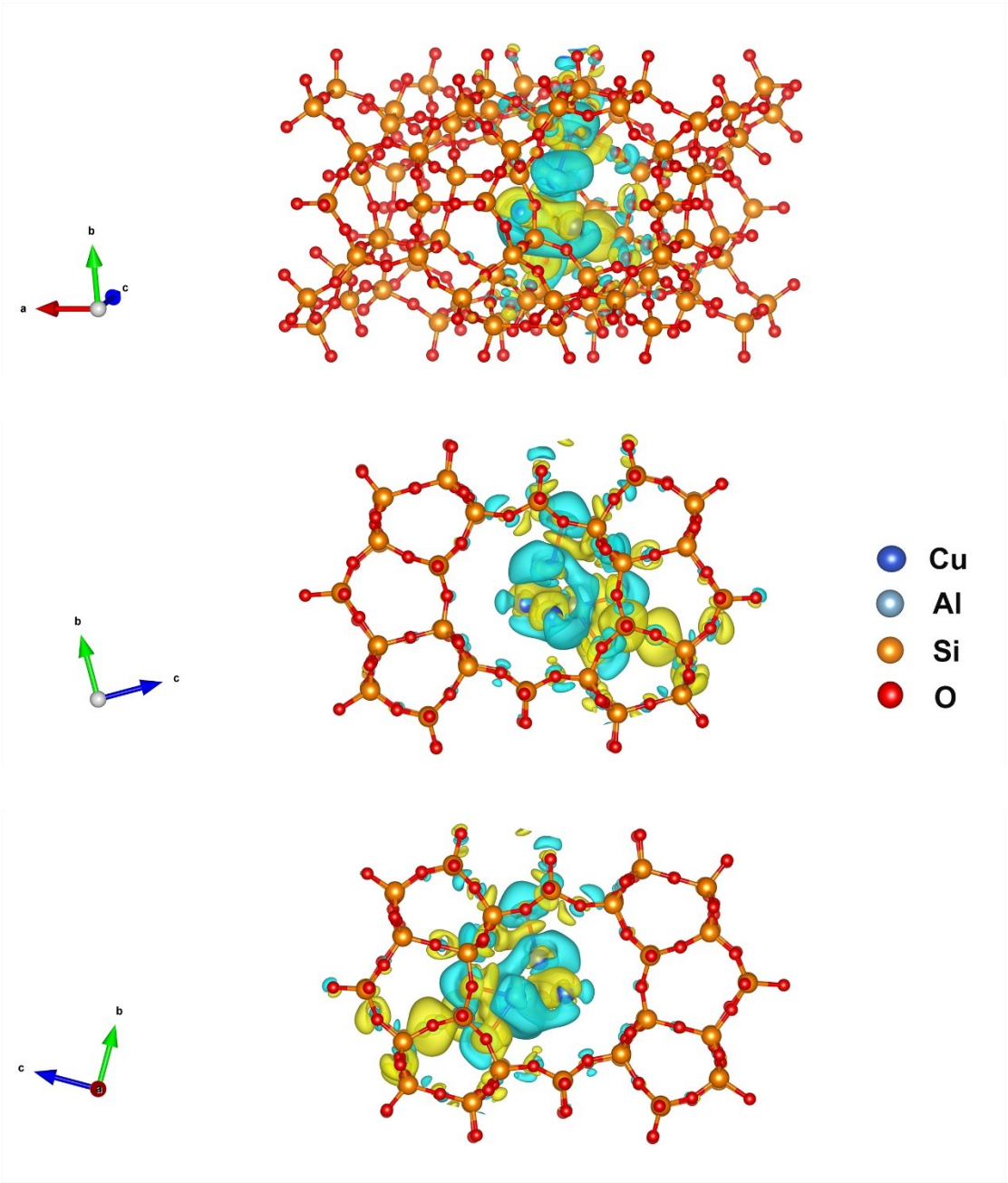

Figure S13. Differential charge density diagram of Cu-MFI

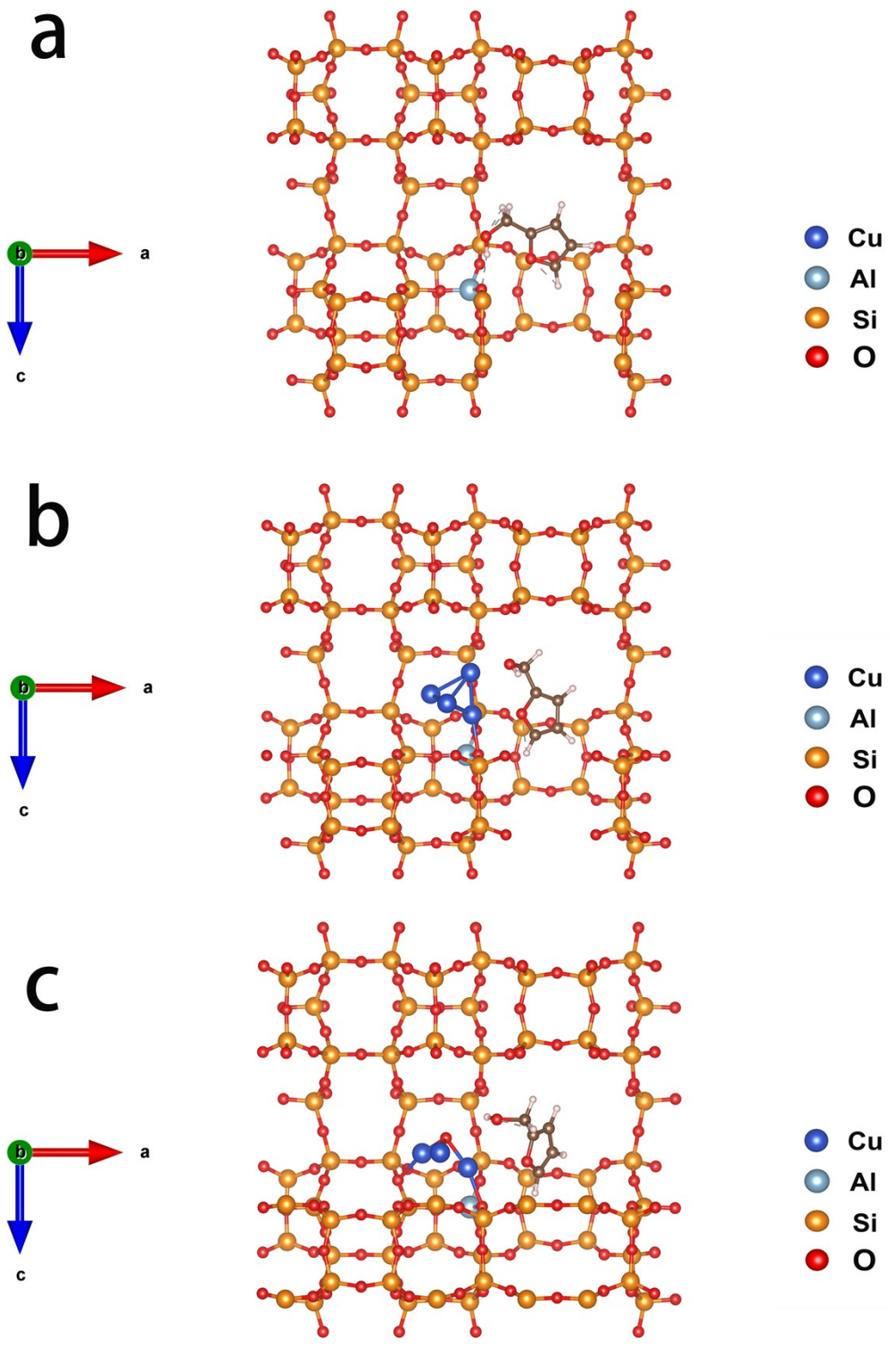

Figure S14. The adsorption configurations of FFA on different materials (section view). (a): FFA-MFI, (b): FFA-Cu, and (c): FFA-Cu_2O

Table S1. The selectivity ratio of 1,5-PDO/1,2-PDO in the literature

Feed	Catalyst	Batch/ Flow	T (℃)	P (MPa)	RT[b]/ WHSV[c]	$S_{1,2\text{-PDO}}$	$S_{1,5\text{-PDO}}$	$S_{1,5\text{-PDO}}/S_{1,2\text{-PDO}}$	Ref
FFA	Cu/Al_2O_3	Batch	140	8.0	8 h	48.6%	22.7%	0.47	[10]
FFA	$Cu/LaCoO_3$	Batch	140	6.0	2 h	15.2%	40.3%	2.65	[11]
FFA	Cu-Co-Al	Batch	160	4.0	2 h	16.1%	41.6%	2.58	[12]
FFA	$Cu\text{-}Mg_3AlO_{4.5}$	Batch	140	6.0	24 h	51.2%	28.8%	0.56	[13]
FFA	Pt/CeO_2	Batch	170	1.0	1.5 h	65.0%	8.0%	0.12	[14]
FFA	Pt/CeO_2	Batch	165	2.0	12 h	77.0%	7.0%	0.09	[15]
FFA	Pt/MgAlOx	Flow	200	3.0	0.12 h^{-1}	86.0%	5.0%	0.06	[16]
FFA	Pt/Co_2AlO_4	Batch	140	1.5	24 h	16.2%	34.9%	2.15	[17]
FA[a]	CuMgAlO	Batch	150	6.0	6 h	55.2%	28.5%	0.52	[18]
FFA	**Cu/MFI**	**Flow**	**160**	**2.5**	**0.19 h^{-1}**	**16.0%**	**69.2%**	**4.33**	**This work**

(1) [a]FA: furfural

(2) [b]RT: reaction time in batch

(3) [c]WHSV: Weight Hour Space Velocity, h^{-1}

Table S2. The proportions of copper valence state calculated by XPS and XAES

catalyst	**Cu^{2+} %**	**Cu^{+} %**	**Cu^{0} %**
Si-10Cu-300R	29.77	44.60	25.63
Si-10Cu-H	7.71	30.10	62.19

Table S3. The effect of reaction temperature on ratio of 1,5-PDO/1,2-PDO selectivity

selectivity	**80℃**	**100℃**	**120℃**	**140℃**	**160℃**	**180℃**	**200℃**	**240℃**
1,5-PDO	36.1%	61.6%	69.7%	69.6%	69.2%	60.0%	56.2%	23.3%
1,2-PDO	0.20%	3.2%	9.6%	12.8%	16.0%	1.8%	1.2%	1.8%
1,5-PDO/ 1,2-PDO	180.5	19.3	7.3	5.4	4.3	33.3	46.8	12.9

Table S4. The effect of reaction pressure on ratio of 1,5-PDO/1,2-PDO selectivity

selectivity	**1.0 MPa**	**2.0 MPa**	**3.0 MPa**	**4.0 MPa**
1,5-PDO	61.6%	74.5%	73.7%	70.6%
1,2-PDO	6.0%	11.2%	11.6%	12.7%
1,5-PDO/1,2-PDO	10.3	6.7	6.4	5.6

Table S5. the bader charge of Cu-MFI

atom	bader	
Cu	10.9	11
Cu	10.96	11
Cu	10.72	11
Cu	10.61	11

Table S6. the bader charge of Cu_2O-MFI

atom	bader	
Cu	10.44	11
Cu	10.40	11
Cu	10.48	11

The bader analysis of Cu-MFI shows that the valence electrons of four Cu atoms are 10.90,10.96,10.72,10.61, respectively. Except for the Cu atom coordinated with MFI, the coordination of the other three Cu atoms is closer to the zero-valence state of metal Cu. But in Cu_2O-MFI, the valence electrons of Cu are 10.44, 10.40 and 10.48, respectively. It can be considered that there are 0.5 valence electrons for bonding and the valence state becomes +1.

References

[1] Z. Huang, F. Cui, H. Kang, J. Chen, X. Zhang, C. Xia, *Chem. Mater.* **2008**, 20, 5090-5099.

[2] J. Pang, M. Zheng, C. Wang, X. Yang, H. Liu, X. Liu, J. Sun, Y. Wang, T. Zhang, *ACS Catal.* **2020**, 10, 13624-13629.

[3] R. Fan, Y. Zhang, Z. Hu, C. Chen, T. Shi, L. Zheng, H. Zhang, J. Zhu, H. Zhao, G. Wang, *Nano Res.* **2021**, 14, 4601-4609.

[4] Y. Zhao, Z. Guo, H. Zhang, B. Peng, Y. Xu, Y. Wang, J. Zhang, Y. Xu, S. Wang, X. Ma, *J. Catal.* **2018**, 357, 223-237.

[5] W. Ding, G. D. Meitzner, D. O. Marler, E. Iglesia, *The Journal of Physical Chemistry B*. **2001**, 105, 3928-3936.

[6] I. Julian, J. L. Hueso, N. Lara, A. Solé-Daurá, J. M. Poblet, S. G. Mitchell, R. Mallada, J. Santamaría, *Catal. Sci. Technol.* **2019**, 9, 5927-5942.

[7] P. Cao, L. Lin, H. Qi, R. Chen, Z. Wu, N. Li, T. Zhang, W. Luo, *ACS Catal.* **2021**, 11, 10246-10256.

[8] A. M. Abdel-Mageed, B. Rungtaweevoranit, M. Parlinska-Wojtan, X. Pei, O. M. Yaghi, R. J. Behm, *J. Am. Chem. Soc.* **2019**, 141, 5201-5210.

[9] G. T. Palomino, S. Bordiga, A. Zecchina, G. L. Marra, C. Lamberti, *The Journal of Physical Chemistry B*. **2000**, 104, 8641-8651.

[10] H. Liu, Z. Huang, H. Kang, C. Xia, J. Chen, *Chinese J. Catal.* **2016**, 37, 700-710.

[11] Fangfang Gao, H. Liu, X. Hu, J. Chen, Z. Huang, C. Xia, *Chinese J. Catal.* **2018**, 39, 1711-1723.

[12] T. P. Sulmonetti, B. Hu, S. Lee, P. K. Agrawal, C. W. Jones, *ACS Sustain. Chem. Eng.* **2017**, 5, 8959-8969.

[13] H. Liu, Z. Huang, F. Zhao, F. Cui, X. Li, C. Xia, J. Chen, *Catal. Sci. Technol.* **2016**, 6, 668-671.

[14] R. Ma, X. Wu, T. Tong, Z. Shao, Y. Wang, X. Liu, Q. Xia, X. Gong, *ACS Catal.* **2017**, 7, 333-337.

[15] T. Tong, X. Liu, Y. Guo, M. Norouzi Banis, Y. Hu, Y. Wang, *J. Catal.* **2018**, 365, 420-428.

[16] Y. Zhu, W. Zhao, J. Zhang, Z. An, X. Ma, Z. Zhang, Y. Jiang, L. Zheng, X. Shu, H. Song, et al., *ACS Catal.* **2020**, 10, 8032-8041.

[17] W. Xu, H. Wang, X. Liu, J. Ren, Y. Wang, G. Lu, *Chem. Commun.* **2011**, 47, 3924.

[18] X. Fu, X. Ren, J. Shen, Y. Jiang, Y. Wang, Y. Orooji, W. Xu, J. Liang, *Molecular Catalysis*. **2021**, 499, 111298.